

PPCR: Learning Pyramid Pixel Context Recalibration Module for Medical Image Classification

Xiaoqing Zhang¹ Zunjie Xiao¹ Xiao Wu¹ Jiansheng Fang¹ Junyong Shen¹
 Yan Hu¹ Risa Higashita^{1,2}
 Jiang Liu¹ *

¹Research Institute of Trustworthy Autonomous Systems and Department of Computer Science and Engineering, Southern University of Science and Technology, Shenzhen, China

²Tomey Corporation, Japan

Abstract

Spatial attention mechanism has been widely incorporated into deep convolutional neural networks (CNNs) via long-range dependency capturing, significantly lifting the performance in computer vision, but it may perform poorly in medical imaging. Unfortunately, existing efforts are often unaware that long-range dependency capturing has limitations in highlighting subtle lesion regions, neglecting to exploit the potential of multi-scale pixel context information to improve the representational capability of CNNs. In this paper, we propose a practical yet lightweight architectural unit, Pyramid Pixel Context Recalibration (PPCR) module, which exploits multi-scale pixel context information to recalibrate pixel position in a pixel-independent manner adaptively. PPCR first designs a cross-channel pyramid pooling to aggregate multi-scale pixel context information, then eliminates the inconsistency among them by the well-designed pixel normalization, and finally estimates per pixel attention weight via a pixel context integration. PPCR can be flexibly plugged into modern CNNs with negligible overhead. Extensive experiments on five medical image datasets and CIFAR benchmarks empirically demonstrate the superiority and generalization of PPCR over state-of-the-art attention methods. The in-depth analyses explain the inherent behavior of PPCR in the decision-making process, improving the interpretability of CNNs.

1. Introduction

Attention mechanism has achieved remarkable success in a variety of computer vision tasks, [7, 12, 13, 25, 39], e.g., object detection, instance segmentation, and image classification. The core idea of the attention mechanism is to al-



Figure 1. Pixel attention weight maps generated by NL [39], GC [3], EA [12], and PPCR at the high stage of ResNet18 for skin disease, blinding disease, and retinal disease based on three medical image modalities: dermatoscopic image, fundus image, and optical coherence tomography (OCT) image. Clearly, our method is more capable of emphasizing subtle lesion regions than state-of-the-art spatial attention methods.

low deep convolutional neural networks (CNNs) to focus on the informative regions and ignore redundant ones. One of the most representative works is the non-local network (NLNet) [39], which belongs to the spatial attention method by explicitly capturing long-range dependencies between pixel positions via a self-attention mechanism. Following the self-attention mechanism used in NLNet, researchers are dedicated to improving self-mechanism design for capturing more sophisticated long-range dependencies among pixel positions [8, 22, 31, 47]. Although self-attention based spatial attention methods have achieved surpassing performance in a variety of natural image-based tasks, they may not perform well on medical image analysis tasks [33].

In seeking answers to this phenomenon, we have gained insights as follows: (1) **Long-Range Dependency Capturing.** Self-attention mechanism commonly captures long-

*Corresponding author

range dependencies across all pixel positions to learn such a pixel position correlation, inevitably introducing redundant position information from other pixel positions. The negative influences of redundant position information on natural image-based tasks can be ignored, because object regions in natural images are discriminative, which is easily highlighted by long-range dependency capturing. In contrast, lesion regions in medical images are subtle. That is, pixel context difference between redundant regions and lesion regions is obscure [14, 15], which is difficult to emphasize lesion regions through modeling long-range dependency. This is mainly because redundant position information significantly negatively influences distinguishing lesion regions and redundant regions. (2) **Pixel Context Aggregation.** Channel attention methods have aggregated multi-scale spatial context information to improve the performance by using spatial pyramid pooling method [11, 21, 27]. However, existing spatial attention methods only have utilized pointwise convolution ($\text{Conv}1 \times 1$) [39], or individual cross-channel pooling (CP) [4] methods to aggregate single-scale pixel context information along the channel axis, often ignoring the effects of multi-scale pixel context information aggregation. According to our extensive literature survey, we have found that no spatial attention method has exploited the potential of multi-scale pixel context information to improve its representational ability.

Based on above systematical analysis, this paper is really curious to find out: (1) *Can one learn an alternative method to highlight informative pixel positions and suppress trivial ones without capturing long-range dependency among pixel positions in spatial attention?* (2) *Can we incorporate **multi-scale pixel context** information into spatial attention design to improve the performance and interpretability of CNNs?*

To answer these two questions, we proposed a novel yet lightweight architectural unit, Pyramid Pixel Context Recalibration (PPCR) module, which explicitly integrates multi-scale pixel context information into CNN representations through a form of pixel-independent context recalibration. Our PPCR consists of a triplet of components: *Cross-Channel Pyramid Pooling*, *Pixel Normalization*, and *Pixel Context Integration*. To the best of our knowledge, this paper is the first to design a *Cross-Channel Pyramid Pooling* to aggregate multi-scale pixel context information at the same pixel positions through different cross-channel scales at the channel dimension. Note that a pixel position involves multi-scale pixel context, and only specific pixel context plays a significant role. Then, *Pixel Normalization* is developed to eliminate the significant fluctuation of multi-scale pixel context distribution per pixel position, which is different from previous normalization methods performs the pixel context statistics at the feature maps. It is followed by *Pixel Context Integration*, which adaptively fuses

normalized multi-scale pixel context information to produce pixel attention weights via pixel-level operation. The pixel attention weights are finally supposed to recalibrate per pixel position to emphasize or ignore their information. Our PPCR only increases negligible computational cost and few parameters, seamlessly plugged into modern CNNs and trained end-to-end.

To demonstrate the effectiveness and efficiency of our method, we conduct extensive experiments on five medical image datasets of two high-resolution datasets and three low-resolution datasets. The results show that our method is superior to state-of-the-art (SOTA) attention methods with less model complexity. Furthermore, we also provide compelling results on CIFAR benchmarks, proving its generalization capability on natural images. Beyond the practical improvements, we empirically analyze the effects of the pixel level recalibration on emphasizing significant pixel positions and redundant ones through visual analysis and ablation study: it controls the relative contributions of multi-scale pixel context information and pixel normalization, which is beneficial to improve the interpretability of CNNs in the decision-making process. Figure 1 provides the generated pixel attention weight maps of PPCR and SOTA attention methods, showing that our method is more capable of locating significant pixel positions accurately than others, agreeing with the clinician’s diagnosis process. We hope our efficient and lightweight design sheds light on future research of attention methods.

In summary, the main contributions of this paper are as follows:

- We propose a pyramid pixel context recalibration module which improves the representational capability of CNNs by combining multi-scale pixel context information and pixel normalization. In particular, this is the first to develop a cross-channel pyramid pooling method to aggregate and exploit multi-scale pixel context information to boost the performance of the spatial attention method. Additionally, we design a pixel normalization method to eliminate the inconsistency of multi-scale pixel context information per-pixel position.
- We conduct comprehensive experiments on five medical image datasets and CIFAR datasets consistently to demonstrate the superiority and generalization capability over SOTA attention methods.
- Visual analysis and ablation study are implemented to interpret the inherent decision-making behavior of our PPCR, conducting to enhancing the interpretability of a CNN.

2. Related Work

Pyramid Pooling. Pyramid pooling is a widely-acknowledged technique to extract multi-scale context information [27, 29, 42, 47]. Mainly, spatial pyramid pooling has been widely utilized in various tasks, e.g., image classification, semantic segmentation, and object detection. He et al. [16] present spatial pyramid pooling to obtain multi-scale spatial context information for image classification. Gu et al. [10] propose spatial pyramid pooling for semantic segmentation. Guo et al. [11] propose spatial pyramid attention (SPA) module by incorporating spatial pyramid pooling for image classification. Unlike existing works that apply spatial pyramid pooling to extract multi-scale spatial context information for channel attention methods, we propose a cross-channel pyramid pooling to extract multi-scale pixel context information for spatial attention methods, which has not been studied before.

Normalization. Batch normalization (BN) [24] is a pioneered technique that normalizes the statistics along the batch axis to stabilize the intermediate feature distribution of hidden layers, allowing deep neural networks to train faster yet fluctuate smaller. Additionally, the property of batch size in BN dramatically affects the network performance when reducing batch size due to inaccurate batch statistics estimation. Several normalization methods have been proposed to tackle this issue [1, 9, 32, 40, 41]. Layer normalization (LN) [1] computes the statistics along the channel axis, and instance normalization (IN) [38] performs the BN-like normalization operator per intermediate feature map. Weight normalization (WN) [35] normalizes the filter weights. Group normalization (GN) [41] divides feature maps into several groups and then computes the statistics per group. The design of our PPCR is motivated by LN. Instead of stabilizing all pixel context features from feature maps along the channel axis, we propose a pixel normalization to normalize pixel context features along the channel axis at the same pixel positions. This is mainly because PPCR is a spatial attention method which aims to emphasize significant pixel positions and suppress trivial ones in a pixel-independent manner.

Attention Mechanism. The current research directions of attention mechanism can be roughly divided into three categories [7, 13, 23, 28, 34, 36, 44, 46]: channel attention, spatial attention, and combination. Squeeze-and-excitation (SE) [25] is one of the successful channel attentions, which captures long-range dependencies among channels. Since PPCR is a spatial attention module, this paper briefly surveyed spatial attention modules. Gather-excite (GE) [19] and coordinate attention (CA) [18] learn long-range spatial context information to boost the performance of CNNs. Recently, self-attention mechanism and its variants [2, 3, 5, 12, 45] dominates the spatial attention research due to their powerful capability in modeling lang-

range dependencies among all pixel positions. For instance, global context network (GCNet) [3] utilizes a self-attention mechanism to construct a global context (GC) block. However, most existing spatial attention methods capture long-range dependencies among all pixel positions, which is skilled at highlighting concentrative object regions in natural images but is poor at learning subtle lesion regions in medical images.

Different from these methods are dedicated to designing self-attention-based spatial attention modules, our method designs a more efficient yet lightweight way to highlight or suppress pixel positions in a pixel-independent manner by incorporating multi-scale pixel context information.

3. Pyramid Pixel Context Recalibration Module

Given the intermediate feature maps $X \in R^{C \times H \times W}$, PPCR generates the pixel attention weight map $G \in R^{1 \times H \times W}$, where C, H and W indicate the number of channels, height and width of feature maps accordingly. As illustrated in Figure 2, our method is abstracted by the following three components: *Cross-Channel Pyramid Pooling*, *Pixel Normalization*, and *Pixel Context Integration*.

3.1. Cross-Channel Pyramid Pooling

Spatial pyramid pooling is often used in channel attention methods to aggregate multi-scale spatial context information from multi-scale spatial regions, significantly improving performance. However, recent spatial attention methods only aggregate single-scale pixel context information and have not yet exploited the potential of multi-scale pixel context information. This paper is the first to propose a cross-channel pyramid pooling (CCPP) method to aggregate multi-scale pixel context information of all pixel positions from cross-channel scales. Sophisticated CCPP design can be used to boost performance further, but this is not the key goal of this paper. Thus, we simply employ an averaged CCPP to aggregate the multi-scale pixel context features of all pixel positions from three different cross-channel scales at the channel dimension. Furthermore, Figure 2(a) provides a visual implementation case of CCPP with three cross-channel scales at a pixel position $x(i, j)$, which can help audiences understand the proposed CCPP visually. The output of multi-scale pixel context description $T \in R^{D \times H \times W}$ (D is the number of pixel context feature maps, and D is equal to 7 in this paper) of all pixel positions through the CCPP can be computed by:

$$T = [CP(X, 1), CP(X, 2), CP(X, 4)], \quad (1)$$

where $CP(X, 1)$, $CP(X, 2)$, and $CP(X, 4)$ indicate one, two, and four pixel context feature maps extracted from three different cross-channel scales. CP indicates the

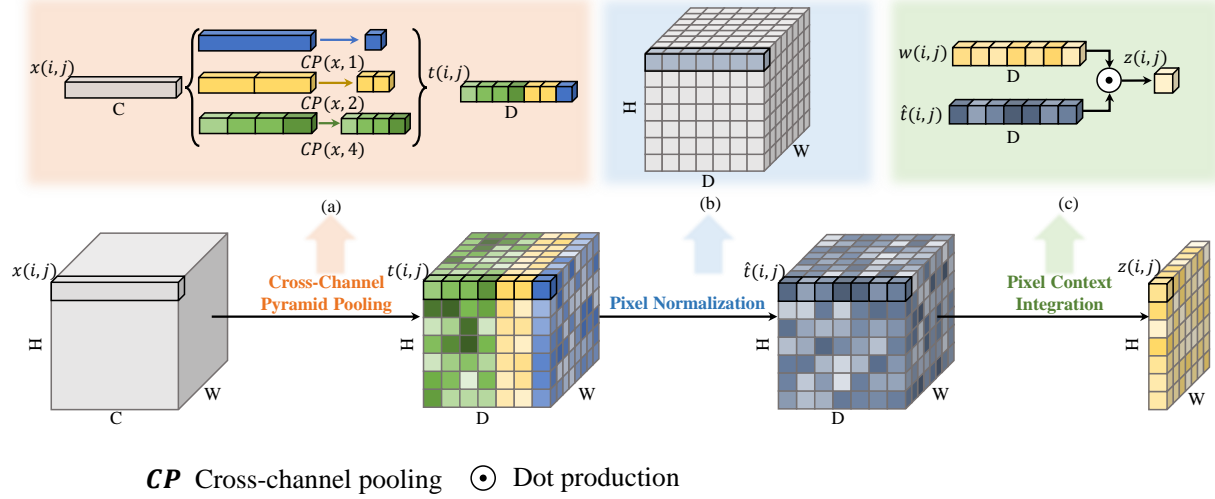


Figure 2. Architecture of the pyramid pixel context recalibration (PPCR) module. Given the intermediate feature maps $X \in R^{C \times H \times W}$, PPCR generates the pixel attention weight map $G \in R^{1 \times H \times W}$.

cross-channel pooling, which performs at per pixel position $x(i, j)$ across channels $K \leq C$ can be computed as follows:

$$\mu(i, j) = \frac{1}{K} \sum_{k=1}^K x(k, i, j), \quad (2)$$

where $\mu(i, j)$ is averaged pixel context feature of $x(i, j)$.

3.2. Pixel Normalization

Existing normalization methods such as LN and BN compute the statistics of pixel context features across the feature map, which can not effectively eliminate the inconsistency of multi-scale pixel context features T at the same pixel positions. To stabilize multi-scale pixel context feature distribution, our PPCR introduces a pixel normalization (PN) to normalize them across all pixel context feature maps at each pixel position, as illustrated in Figure 2(b). For each pixel context $t(d, i, j)$, the PN can be formulated as follows:

$$\hat{t}_{d,i,j} = \frac{t_{d,i,j} - \mu_{(i,j)}^{(t)}}{\delta_{(i,j)}^{(t)}}, \quad (3)$$

where $\hat{t}_{(d,i,j)}$ indicates the normalized multi-scale pixel context at the pixel position (i, j) of for d pixel context feature map. $\mu_{(i,j)}^{(t)}$ and $\delta_{(i,j)}^{(z)}$ are the mean $\mu_{(i,j)}^t$ and standard deviation $\delta_{(i,j)}^{(t)}$ of multi-scale pixel context features at pixel position $t(i, j)$, which can be computed as:

$$\mu_{(i,j)}^t = \frac{1}{D} \sum_{i=1}^D z_{(d,i,j)}, \delta_{(i,j)}^{(t)} = \sqrt{\frac{1}{D} \sum_{i=1}^D (z_{(d,i,j)} - \mu_{(i,j)}^{(t)})^2 + \xi}, \quad (4)$$

where ξ is a very small constant.

3.3. Pixel Context Integration

Following the PN, we define the pixel context integration (PCI) function (as shown in Figure 2(c)) to convert the normalized multi-scale pixel context features $\hat{T} \in R^{D \times H \times W}$ into pixel attention weights G , which can be represented by:

$$G = \sigma(Z), \quad (5)$$

where σ is the sigmoid function as the gating mechanism; $Z \in R^{1 \times H \times W}$ indicates the encoded multi-scale pixel context features, which can be formulated as:

$$Z = W \cdot \hat{T}, \quad (6)$$

where $W \in R^{7 \times H \times W}$ indicates learnable parameters. Finally, the output $Y \in R^{C \times H \times W}$ is computed as follows:

$$Y = G \cdot X. \quad (7)$$

3.4. Complexity Analysis

Our PPCR is supposed to be lightweight in terms of computational cost and parameters. The PCI function determines the additional parameters of PPCR: $\sum_{s=1}^S H_s \cdot W_s \cdot N_s \cdot 7$. S and N_s represent the number of stages and the number of repeated blocks in the s -th stage, which we follow the same definition of stage in [17], H_s and W_s represent the height and width of feature maps in the s -th stage. Therefore, the total number of additional parameters for PPCR is:

$$7 \sum_{s=1}^S N_s \cdot H_s \cdot W_s, \quad (8)$$

which is far less than the total number of parameters for NL: $\frac{2}{r} \sum_{s=1}^S N_s C_s + \sum_{s=1}^S N_s^2$ where r and C_s represent

the reduction ratio and the number of output channels in the s -th stage. According to Eq. 8, the extra parameters of PPCR are determined by the height and width of a feature map, which is different from the extra parameters of channel attention methods determined by the number of channels. Theoretically, our method has parameter advantages over channel attention methods on low-resolution images, which will be verified in experiments. As for computational cost, our PPCR introduces negligible extra computations compared to original network architectures. For example, given a 224×224 pixel image or 28×28 as input, PPCR-ResNet50 shares almost the same computations as ResNet50.

4. Experiments

In this section, we first introduce our experiment setup and then demonstrate the effectiveness and generalization ability of our proposed method on five medical image datasets and CIFAR benchmarks through comparisons to SOTA attention methods. Then, we conduct systematic visual analyses and ablation study to investigate the inherent behavior of PPCR.

4.1. Experiment Setup

In this paper, we use the following SOTA attention methods to demonstrate the effectiveness of PPCR based on five medical datasets, including SE, SPA, CA, SA (CBAM), NL, EA, and GC by adopting two commonly used CNN architectures as backbones: ResNet18 and ResNet50 [17]. Specifically, SA, NL, EA, and GC are spatial attention methods involving local-range and long-range dependency modeling, which are able to verify the superiority of our method comprehensively.

These methods are implemented by the PyTorch package and use SGD optimizer with default settings during the training process. The initial learning rate is decreased by a factor of 10 every 40 epochs. We set batch size and epochs to 32 and 150 accordingly and run all methods on two TITAN V NVIDIA GPUs under the same experiment settings. Furthermore, five commonly-accepted evaluation metrics are adopted to evaluate the performance and model complexity of PPCR, SOTA attention methods, and baselines: accuracy (ACC), area under the ROC curve (AUC), F1, parameters (Params.), and GFLOPs.

4.2. Medical Image Classification Results

ISIC2018. ISIC2018 [37] is a publicly available skin lesion dataset with 10,015 images of seven different labels. This paper uses the same data augmentation strategy in literature [30]. We split the dataset into training, validation, and testing datasets [30] and then resize all images into 224×224 pixels as input image size for the network. The classification results on the testing dataset are adopted for comparison, and the validation dataset is used to choose

the best-trained model. The following experiments adopt the same settings. Listed as in Table 1(Left), PPCR generally performs better between the performance and model complexity than other SOTA attention methods by taking ResNet18 and ResNet50 as backbones. Remarkably, PPCR outperforms CA by absolute over **2.60%** in accuracy under ResNet50, although CA is 1.3% larger in computation cost and **16%** in parameters. Compared with SOTA counterparts (e.g., GC, NL and EA), PPCR consistently obtains over **3.1%** and **2.6%** gains of accuracy and F1 accordingly while benefiting fewer computational costs and parameters. For example, NL is **96%** larger in parameters and **90%** larger in computational cost than PPCR based on ResNet50. We also observe that PPCR outperforms SPA by **3.65%** of accuracy, **5.06%** of AUC, and **7.6%** of F1 accordingly based on ResNet50, which demonstrate the superiority of multi-scale pixel context aggregation via CCPP for spatial attention mechanism compared to multi-scale spatial context aggregation for channel attention mechanism via spatial pyramid pooling.

Fundus-Isee. Fundus-iSee is a fundus image dataset with 10,000 images. Fundus-iSee is a fundus image dataset with 10,000 images. It contains four different ocular diseases: age-related macular degeneration (720), diabetic retinopathy (270), glaucoma (450), myopia (790), and normal (7,770). We follow the same data augmentation and dataset splitting methods in literature [6]. The input size of fundus images is resized into 224×224 . The results show that PPCR consistently improves performance over comparable attention methods under fewer budgets. PPCR improves two backbones over 2.25% of F1 by using almost the same model complexity. At the same time, NL, GC, and EA perform worse than these two backbones, demonstrating that our PPCR is more able to locate significant subtle lesion regions than these self-attention-based spatial attention methods.

MedMNIST Datasets. MedMNIST is an MNIST-like benchmark for medical image classification [43], containing 15 medical image datasets. In this paper, we use three MedMNIST datasets to further demonstrate the efficiency and effectiveness of our PPCR on low-resolution medical image datasets: OCTMNIST, RetinaMNIST, and BreastMNIST. OCTMNIST comprises 109,309 OCT images of four retinal diseases. RetinaMNIST contains 1,600 retina fundus images of five diabetic retinopathy severity levels. BreastMNIST has 780 breast ultrasound images of two labels. The image size of these three datasets is 28×28 . Moreover, data augmentation and dataset splitting methods are adopted from literature [43] for a fair comparison. According to Table 2, PPCR achieves a better trade-off between effectiveness and efficiency than SOTA attention methods on three MedMNIST datasets. It is worth noting that PPCR outperforms NL by absolute over **16%** on the

Method	ISIC2018			Fundus-Isee			Params	GFLOPs
	ACC	AUC	F1	ACC	AUC	F1		
ResNet18	78.65	86.31	76.73	79.23	70.36	71.19	11.18M	1.820
+SE [25]	77.60	89.67	74.57	79.03	69.54	71.33	11.27M	1.821
+SPA [11]	79.17	89.66	77.37	79.13	70.70	71.40	12.14M	1.822
+CA [18]	77.60	89.62	76.27	79.54	69.07	72.38	11.32M	1.822
+NL [39]	73.96	86.76	71.32	78.02	67.75	69.30	11.97M	1.935
+GC [3]	77.08	86.64	74.49	79.03	71.62	71.35	11.36M	1.819
+EA [12]	70.31	86.66	62.73	78.93	64.80	71.55	11.43M	1.915
+PPCR	80.21	91.81	77.11	80.34	71.88	73.44	11.18M	1.820
ResNet50	72.92	86.93	69.22	78.33	66.08	69.50	23.52M	4.116
+SE [25]	73.96	85.64	68.80	77.52	64.40	67.70	26.05M	4.118
+SPA [11]	74.48	84.21	69.84	78.23	67.12	69.27	51.19M	4.153
+CA [18]	75.52	89.25	73.61	78.73	66.45	70.71	27.33M	4.171
+NL [39]	65.63	67.22	54.27	77.52	57.81	67.70	46.17M	7.815
+GC [3]	68.23	81.07	58.82	77.92	65.38	68.24	28.58M	4.120
+EA [12]	72.92	87.36	70.81	78.83	66.83	72.05	25.46M	4.816
+PPCR	78.13	89.27	77.44	79.44	69.22	72.34	23.52M	4.116

Table 1. Performance comparison of different attention methods on two medical image datasets (ISIC2018 and Fundus-Isee) in terms of accuracy, AUC, F1, parameters, and GFLOPs.

Method	OCTMNIST			RetinaMNIST			BreastMNIST			Params	GFLOPs
	ACC	AUC	F1	ACC	AUC	F1	ACC	AUC	F1		
ResNet18	76.20	93.89	73.61	52.00	68.96	48.52	85.90	87.93	85.39	11.17M	0.458
+SE [25]	77.50	94.89	75.14	51.00	67.62	50.95	85.26	88.01	84.65	11.31M	0.458
+SPA [11]	78.60	94.74	76.91	52.00	73.59	49.54	82.05	86.77	81.59	12.13M	0.459
+CA [18]	78.70	94.20	76.27	50.00	74.31	47.65	85.26	87.81	86.97	11.31M	0.459
+NL [39]	75.60	94.11	72.26	51.75	74.19	50.04	82.69	87.98	83.08	11.96M	0.489
+GC [3]	73.20	93.61	68.84	51.50	65.77	48.96	82.05	81.89	86.85	11.35M	0.458
+EA [12]	71.60	93.97	65.88	49.25	72.44	43.40	73.72	54.75	63.19	11.42M	0.482
+PPCR	79.80	96.33	77.79	53.00	73.63	50.01	87.20	88.89	86.97	11.17M	0.458
ResNet50	75.40	92.86	72.04	51.50	69.36	50.56	83.33	88.24	83.30	23.51M	1.053
+SE [25]	72.50	92.69	67.69	47.75	67.29	47.22	84.62	86.90	84.36	26.24M	1.057
+SPA [11]	77.20	95.04	74.61	50.25	66.36	47.63	82.05	88.16	82.59	51.18M	1.085
+CA [18]	77.60	93.71	74.58	51.00	69.34	50.37	84.62	89.22	84.36	27.32M	1.083
+NL [39]	65.80	90.40	58.78	48.00	65.18	39.70	76.28	70.38	71.37	46.16M	2.033
+GC [3]	67.70	90.41	60.51	52.75	66.35	49.33	80.77	75.56	77.84	28.57M	1.060
+EA [12]	73.00	91.90	68.36	49.00	70.92	43.84	73.71	63.31	68.89	25.44M	1.223
+PPCR	81.90	95.38	79.97	53.25	73.68	50.51	88.46	89.35	84.37	23.51M	1.053

Table 2. Performance comparison of different attention methods on three MedMNIST datasets (OCTMNIST, RetinaMNIST, and BreastMNIST) in terms of accuracy, AUC, F1, parameters, and GFLOPs.

OCTMNIST dataset by taking ResNet50 as the backbone, although NL is **96%** larger in parameters.

Moreover, The results in Table 1 and Table 2 demonstrate that PPCR effectively leverages the potential of multi-scale pixel context information and pixel normalization to dynamically re-estimate the relative importance of each pixel position in a pixel-independent manner, agreeing with

our expectation.

4.3. Visual Analysis and Interpretation

Attention Weight Visualization. Figure 3 plots pixel attention weight feature maps and pixel attention weight distributions of PPCR at three stages: low (Stage_1), middle (Stage_2), and high (Stage_3) of PPCR-ResNet18 on

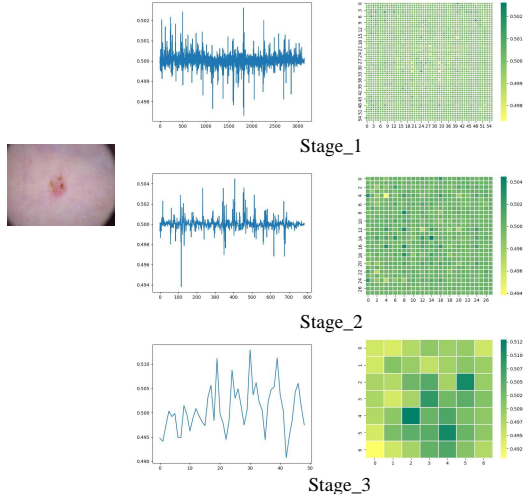


Figure 3. The pixel attention weight feature maps and pixel attention weight distributions of PPCR-ResNet18 at three different stages. The dataset is ISIC2018.

the ISIC2018 dataset. We find that when the network goes deeper, attention weight differences among pixel positions become more evident, proving that PPCR is capable of distinguishing subtle lesion regions efficiently. Furthermore, Figure 1 (first row) provides pixel attention weight feature maps of NL, GC, EA, and PPCR at the high stage on the ISIC2018 dataset. We find that compared with attention weight differences among pixel positions for NL, GC, and EA, attention weight difference among pixel positions is more apparent. More visual analysis of pixel attention weight feature maps and pixel attention weight distributions of NL, GC, EA, and PPCR are provided in the supplementary materials. The visual analyses demonstrate that PPCR takes advantage of multi-scale pixel context information and pixel normalization in a pixel-independent manner rather than a long-range capturing manner through comparisons to NL, GC, and EA.

Multi-Scale Pixel Context Value Visualization. Figure 4(a) presents the multi-scale pixel context feature distributions before and after PN at the high stage of PPCR-ResNet18 on ISIC2018 dataset. We observe that multi-scale pixel context feature distributions differ, indicating that they play varying significance in PPCR. The fluctuations of multi-scale pixel context feature distribution after PN are smaller than before PN, proving that PN can effectively address the inconsistency among multi-scale pixel context features. More details are provided in the supplementary materials.

Multi-Scale Pixel Context Weight Visualization. Figure 4(b) offers multi-scale pixel context weight distributions of PPCR-ResNet18 at three stages. We find a significant difference between multi-scale pixel context weight distri-

Cross-channel scale	ACC	F1
1	78.13	75.95
2	61.46	49.72
3	80.21	77.11
4	78.13	76.76

Table 3. Results of different cross-channel scales with PPCR-ResNet18 on the ISIC2018 testing dataset.

Normalization	ACC	F1
Original	78.65	76.53
BN	77.60	75.62
IN	78.65	77.14
LN	77.60	74.46
PN (ours)	80.21	77.11

Table 4. Results of different normalization methods with PPCR-ResNet18 on ISIC2018 testing dataset.

butions, proving our PPCR adaptively sets relative weights to multi-scale pixel contexts, guiding CNNs to emphasize or suppress significant pixel positions. More details of pixel context weight distributions along the pixel position are provided in the supplementary materials.

4.4. Ablation Study

In this section, we perform a series of ablation experiments to examine which factors affect the effectiveness of PPCR. Throughout the ablation study, we adopt ResNet18 as a backbone architecture and recognize skin disease on ISIC2018 dataset by following the same experiment setting in Section 4.1 and 4.2.

Number of Cross-Channel Scales. Table 3 provides results of four different cross-channel scales used in CCPP for our method. 1 denotes one cross-channel scale: $1 \times H \times W$, 2 denotes two cross-channel scales: $1 \times H \times W$, and $2 \times H \times W$, and so on. PPCR is sensitive to the variation of cross-channel scale numbers, mainly because mean and variance change with the number of multi-scale pixel context features per pixel position, indicating they play different roles. When cross-channel scale=3, it performs better than other settings adopted in this paper.

Normalization. To investigate the effects of the normalization methods on the PPCR module, this paper compares PN with BN, IN, LN, and the original (without any normalization operation). According to Table 4, we see that the performance of PN is better than the other three normalization methods and the original, demonstrating the advantages of PN in eliminating the inconsistency of pixel context feature distribution at the same pixel positions.

Initialization. Table 5 lists the results of initialization

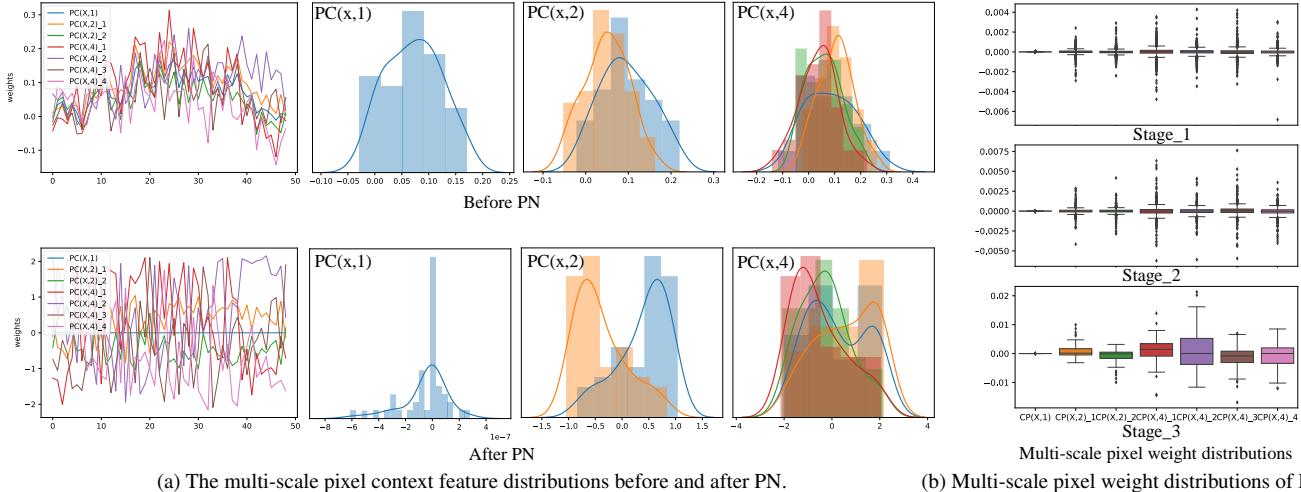


Figure 4. The multi-scale pixel context feature distributions before and after PN at the high stage (a). Multi-scale pixel weight distributions of PPCR at three stages. The dataset is ISIC2018 and the backbone is ResNet18 (b).

Initialization		
W	ACC	F1
0	80.21	77.11
1	79.69	77.04

Table 5. Results of two initializations with PPCR-ResNet18 on ISIC2018 testing dataset.

methods for learnable parameters W . We find it more appropriate to initially set W to 0 rather than 1, referring to the classification results. This initialization also conduces to PPCR biasedly to give the higher pixel attention weights for informative pixel positions, as shown in Figure 1 and Figure 2.

Validation on CIFAR Benchmarks. CIFAR benchmarks contain CIFAR-10 and CIFAR-100 [26], which are colored natural images of 32×32 pixels. Training and testing datasets provide 50,000 and 10,000 images accordingly. We follow the standard practice [20] to augment image data by padding zero to four pixels and randomly cropping them to the original size. As listed in Table 6, PPCR significantly improves the performance on CIFAR benchmarks with minimal parameter and computational cost increment, which proves the generalization ability of PPCR is not constrained to medical image datasets.

5. Conclusion

In this paper, we propose an efficient yet lightweight pyramid pixel context recalibration module (PPCR) to dynamically estimate the relative significance of each pixel position in a pixel-independent manner based on multi-

Method	CIFAR-10	CIFAR-100	Params	GFLOPs
	ACC	ACC		
ResNet18	93.02	74.56	11.22M	0.557
+SE [25]	94.84	75.19	11.32M	0.557
+SPA [11]	95.00	75.56	12.18M	0.557
+CA [18]	95.21	77.73	11.36M	0.558
+NL [39]	93.38	71.97	12.01M	0.595
+GC [3]	95.38	77.53	11.40M	0.557
+EA [12]	93.16	72.05	11.47M	0.588
+PPCR	95.56	78.70	11.22M	0.557
ResNet50	93.62	78.51	23.71M	1.305
+SE [25]	95.35	79.28	26.24M	1.309
+SPA [11]	94.63	78.21	51.37M	1.338
+CA [18]	95.52	79.45	27.51M	1.340
+NL [39]	94.00	72.15	46.36M	2.515
+GC [3]	95.60	78.37	28.77M	1.312
+EA [12]	93.98	71.85	25.64M	1.536
+PPCR	95.92	79.93	23.71M	1.305

Table 6. Performance comparison of different attention methods on CIFAR benchmarks in terms of accuracy, parameters, and GFLOPs.

scale pixel context features. By incorporating multi-scale pixel context features into feature maps at the pixel level, it improves the representational ability of a CNN efficiently. The experimental results demonstrate the effectiveness and generalization ability of our PPCR through comparisons to SOTA attention methods on both medical image and natural image datasets. Furthermore, we provide visual analyses and ablation study to explain the significance of PPCR in adjusting the relative contribu-

tions of multi-scale pixel context information and pixel normalization, contributing to improving the interpretability of CNNs. In future work, we plan to present more efficient methods to explore multi-scale pixel context, which may provide new insights in spatial attention design.

References

- [1] Jimmy Lei Ba, Jamie Ryan Kiros, and Geoffrey E Hinton. Layer normalization. *arXiv preprint arXiv:1607.06450*, 2016. **3**
- [2] Irwan Bello, Barret Zoph, Ashish Vaswani, Jonathon Shlens, and Quoc V Le. Attention augmented convolutional networks. In *Proceedings of the IEEE/CVF international conference on computer vision*, pages 3286–3295, 2019. **3**
- [3] Yue Cao, Jiarui Xu, Stephen Lin, Fangyun Wei, and Han Hu. Gcnet: Non-local networks meet squeeze-excitation networks and beyond. In *Proceedings of the IEEE/CVF international conference on computer vision workshops*, pages 0–0, 2019. **1, 3, 6, 8**
- [4] Tse-Wei Chen, Motoki Yoshinaga, Hongxing Gao, Wei Tao, Dongchao Wen, Junjie Liu, Kinya Osa, and Masami Kato. Condensation-net: memory-efficient network architecture with cross-channel pooling layers and virtual feature maps. In *Proceedings of the IEEE/CVF Conference on Computer Vision and Pattern Recognition Workshops*, pages 0–0, 2019. **2**
- [5] Xiangxiang Chu, Zhi Tian, Yuqing Wang, Bo Zhang, Haibing Ren, Xiaolin Wei, Huaxia Xia, and Chunhua Shen. Twins: Revisiting the design of spatial attention in vision transformers. *Advances in Neural Information Processing Systems*, 34:9355–9366, 2021. **3**
- [6] Jiansheng Fang, Huazhu Fu, and Jiang Liu. Deep triplet hashing network for case-based medical image retrieval. *Medical Image Analysis*, 69:101981, 2021. **5**
- [7] Jun Fu, Jing Liu, Jie Jiang, Yong Li, Yongjun Bao, and Hanqing Lu. Scene segmentation with dual relation-aware attention network. *IEEE Transactions on Neural Networks and Learning Systems*, 2020. **1, 3**
- [8] Jun Fu, Jing Liu, Haijie Tian, Yong Li, Yongjun Bao, Zhiwei Fang, and Hanqing Lu. Dual attention network for scene segmentation. In *Proceedings of the IEEE/CVF conference on computer vision and pattern recognition*, pages 3146–3154, 2019. **1**
- [9] Shang-Hua Gao, Qi Han, Duo Li, Ming-Ming Cheng, and Pai Peng. Representative batch normalization with feature calibration. In *Proceedings of the IEEE/CVF Conference on Computer Vision and Pattern Recognition*, pages 8669–8679, 2021. **3**
- [10] Zaiwang Gu, Jun Cheng, Huazhu Fu, Kang Zhou, Huaying Hao, Yitian Zhao, Tianyang Zhang, Shenghua Gao, and Jiang Liu. Ce-net: Context encoder network for 2d medical image segmentation. *IEEE transactions on medical imaging*, 38(10):2281–2292, 2019. **3**
- [11] Jingda Guo, Xu Ma, Andrew Sansom, Mara McGuire, Andrew Kalaani, Qi Chen, Sihai Tang, Qing Yang, and Song Fu. Spanet: Spatial pyramid attention network for enhanced image recognition. In *ICME*, pages 1–6. IEEE, 2020. **2, 3, 6, 8**
- [12] Meng-Hao Guo, Zheng-Ning Liu, Tai-Jiang Mu, and Shi-Min Hu. Beyond self-attention: External attention using two linear layers for visual tasks. *IEEE Transactions on Pattern Analysis and Machine Intelligence*, 2022. **1, 3, 6, 8**
- [13] Meng-Hao Guo, Tian-Xing Xu, Jiang-Jiang Liu, Zheng-Ning Liu, Peng-Tao Jiang, Tai-Jiang Mu, Song-Hai Zhang, Ralph R Martin, Ming-Ming Cheng, and Shi-Min Hu. Attention mechanisms in computer vision: A survey. *Computational Visual Media*, pages 1–38, 2022. **1, 3**
- [14] Fatemeh Haghighi, Mohammad Reza Hosseinzadeh Taher, Michael B Gotway, and Jianming Liang. Dira: Discriminative, restorative, and adversarial learning for self-supervised medical image analysis. In *Proceedings of the IEEE/CVF Conference on Computer Vision and Pattern Recognition*, pages 20824–20834, 2022. **2**
- [15] Fatemeh Haghighi, Mohammad Reza Hosseinzadeh Taher, Zongwei Zhou, Michael B Gotway, and Jianming Liang. Transferable visual words: Exploiting the semantics of anatomical patterns for self-supervised learning. *IEEE transactions on medical imaging*, 40(10):2857–2868, 2021. **2**
- [16] Kaiming He, Xiangyu Zhang, Shaoqing Ren, and Jian Sun. Spatial pyramid pooling in deep convolutional networks for visual recognition. *IEEE transactions on pattern analysis and machine intelligence*, 37(9):1904–1916, 2015. **3**
- [17] Kaiming He, Xiangyu Zhang, Shaoqing Ren, and Jian Sun. Deep residual learning for image recognition. In *CVPR*, pages 770–778, 2016. **4, 5**
- [18] Qibin Hou, Daquan Zhou, and Jiashi Feng. Coordinate attention for efficient mobile network design. In *Proceedings of the IEEE/CVF Conference on Computer Vision and Pattern Recognition*, pages 13713–13722, 2021. **3, 6, 8**
- [19] Jie Hu, Li Shen, Samuel Albanie, Gang Sun, and Andrea Vedaldi. Gather-excite: Exploiting feature context in convolutional neural networks. *Advances in neural information processing systems*, 31, 2018. **3**
- [20] Jie Hu, Li Shen, and Gang Sun. Squeeze-and-excitation networks. In *Proceedings of the IEEE conference on computer vision and pattern recognition*, pages 7132–7141, 2018. **8**
- [21] Xuefeng Hu, Zhihan Zhang, Zhenye Jiang, Syomantak Chaudhuri, Zhenheng Yang, and Ram Nevatia. Span: Spatial pyramid attention network for image manipulation localization. In *European conference on computer vision*, pages 312–328. Springer, 2020. **2**
- [22] Zhanchao Huang, Wei Li, Xiang-Gen Xia, Xin Wu, Zhaoquan Cai, and Ran Tao. A novel nonlocal-aware pyramid and multiscale multitask refinement detector for object detection in remote sensing images. *IEEE Transactions on Geoscience and Remote Sensing*, 60:1–20, 2021. **1**
- [23] Zilong Huang, Xinggang Wang, Lichao Huang, Chang Huang, Yunchao Wei, and Wenyu Liu. Ccnet: Criss-cross attention for semantic segmentation. In *Proceedings of the IEEE/CVF international conference on computer vision*, pages 603–612, 2019. **3**
- [24] Sergey Ioffe and Christian Szegedy. Batch normalization: Accelerating deep network training by reducing internal co-

- variate shift. In *International conference on machine learning*, pages 448–456. PMLR, 2015. 3
- [25] Jie, Hu, Li, Shen, Samuel, Albanie, Gang, Sun, Enhua, and Wu. Squeeze-and-excitation networks. *TPAMI*, 2019. 1, 3, 6, 8
- [26] Alex Krizhevsky, Geoffrey Hinton, et al. Learning multiple layers of features from tiny images. 2009. 8
- [27] Hanchao Li, Pengfei Xiong, Jie An, and Lingxue Wang. Pyramid attention network for semantic segmentation. *arXiv preprint arXiv:1805.10180*, 2018. 2, 3
- [28] Xiang Li, Wenhai Wang, Xiaolin Hu, and Jian Yang. Selective kernel networks. In *Proceedings of the IEEE/CVF conference on computer vision and pattern recognition*, pages 510–519, 2019. 3
- [29] Xuhang Lian, Yanwei Pang, Jungong Han, and Jing Pan. Cascaded hierarchical atrous spatial pyramid pooling module for semantic segmentation. *Pattern Recognition*, 110:107622, 2021. 3
- [30] Fengbei Liu, Yu Tian, Yuanhong Chen, Yuyuan Liu, Vasileios Belagiannis, and Gustavo Carneiro. Acpl: Anticurriculum pseudo-labelling for semi-supervised medical image classification. In *Proceedings of the IEEE/CVF Conference on Computer Vision and Pattern Recognition*, pages 20697–20706, 2022. 5
- [31] Yiqun Mei, Yuchen Fan, and Yuqian Zhou. Image super-resolution with non-local sparse attention. In *Proceedings of the IEEE/CVF Conference on Computer Vision and Pattern Recognition*, pages 3517–3526, 2021. 1
- [32] Anthony Ortiz, Caleb Robinson, Dan Morris, Olac Fuentes, Christopher Kiekintveld, Md Mahmudulla Hassan, and Nebojsa Jovic. Local context normalization: Revisiting local normalization. In *Proceedings of the IEEE/CVF Conference on Computer Vision and Pattern Recognition*, pages 11276–11285, 2020. 3
- [33] Adrit Rao, Jongchan Park, Sanghyun Woo, Joon-Young Lee, and Oliver Aalami. Studying the effects of self-attention for medical image analysis. In *Proceedings of the IEEE/CVF International Conference on Computer Vision*, pages 3416–3425, 2021. 1
- [34] Dongsheng Ruan, Jun Wen, Nenggan Zheng, and Min Zheng. Linear context transform block. In *Proceedings of the AAAI Conference on Artificial Intelligence*, volume 34, pages 5553–5560, 2020. 3
- [35] Tim Salimans and Durk P Kingma. Weight normalization: A simple reparameterization to accelerate training of deep neural networks. *Advances in neural information processing systems*, 29, 2016. 3
- [36] Jo Schlemper, Ozan Oktay, Michiel Schaap, Mattias Heinrich, Bernhard Kainz, Ben Glocker, and Daniel Rueckert. Attention gated networks: Learning to leverage salient regions in medical images. *Medical image analysis*, 53:197–207, 2019. 3
- [37] Philipp Tschandl, Cliff Rosendahl, and Harald Kittler. The ham10000 dataset, a large collection of multi-source dermatoscopic images of common pigmented skin lesions. *Scientific data*, 5(1):1–9, 2018. 5
- [38] Dmitry Ulyanov, Andrea Vedaldi, and Victor Lempitsky. Instance normalization: The missing ingredient for fast stylization. *arXiv preprint arXiv:1607.08022*, 2016. 3
- [39] Xiaolong Wang, Ross Girshick, Abhinav Gupta, and Kaiming He. Non-local neural networks. In *Proceedings of the IEEE conference on computer vision and pattern recognition*, pages 7794–7803, 2018. 1, 2, 6, 8
- [40] Jun Wen, Risheng Liu, Nenggan Zheng, Qian Zheng, Zhefeng Gong, and Junsong Yuan. Exploiting local feature patterns for unsupervised domain adaptation. In *Proceedings of the AAAI conference on artificial intelligence*, volume 33, pages 5401–5408, 2019. 3
- [41] Yuxin Wu and Kaiming He. Group normalization. In *Proceedings of the European conference on computer vision (ECCV)*, pages 3–19, 2018. 3
- [42] Yu-Huan Wu, Yun Liu, Xin Zhan, and Ming-Ming Cheng. P2t: Pyramid pooling transformer for scene understanding. *IEEE Transactions on Pattern Analysis and Machine Intelligence*, 2022. 3
- [43] Jiancheng Yang, Rui Shi, Donglai Wei, Zequan Liu, Lin Zhao, Bilian Ke, Hanspeter Pfister, and Bingbing Ni. Medmnist v2: A large-scale lightweight benchmark for 2d and 3d biomedical image classification. *arXiv preprint arXiv:2110.14795*, 2021. 5
- [44] Xiaoqing Zhang, Zunjie Xiao, Huazhu Fu, Yan Hu, Jin Yuan, Yanwu Xu, Risa Higashita, and Jiang Liu. Attention to region: Region-based integration-and-recalibration networks for nuclear cataract classification using as-oct images. *Medical Image Analysis*, page 102499, 2022. 3
- [45] Hengshuang Zhao, Yi Zhang, Shu Liu, Jianping Shi, Chen Change Loy, Dahua Lin, and Jiaya Jia. Psanet: Pointwise spatial attention network for scene parsing. In *Proceedings of the European conference on computer vision (ECCV)*, pages 267–283, 2018. 3
- [46] Sixiao Zheng, Jiachen Lu, Hengshuang Zhao, Xiatian Zhu, Zekun Luo, Yabiao Wang, Yanwei Fu, Jianfeng Feng, Tao Xiang, Philip HS Torr, et al. Rethinking semantic segmentation from a sequence-to-sequence perspective with transformers. In *Proceedings of the IEEE/CVF conference on computer vision and pattern recognition*, pages 6881–6890, 2021. 3
- [47] Zhen Zhu, Mengde Xu, Song Bai, Tengpeng Huang, and Xiang Bai. Asymmetric non-local neural networks for semantic segmentation. In *Proceedings of the IEEE/CVF International Conference on Computer Vision*, pages 593–602, 2019. 1, 3